CP1195, *Shock Compression of Condensed Matter - 2009*,
edited by M. L. Elert, W. T. Buttler, M. D. Furnish, W. W. Anderson, and W. G. Proud
© 2009 American Institute of Physics 978-0-7354-0732-9/09/$25.00

LASER COMPRESSION OF NANOCRYSTALLINE METALS

M. A. Meyers[1], H. N. Jarmakani[1], E. M. Bringa[2], P. Earhart[2], B. A. Remington[2], N. Q. Vo[3] and Y. M. Wang[3]

[1]*University of California, San Diego, La Jolla, CA 92093-0418*
[2]*Lawrence Livermore National Laboratory, Livermore, CA 94550*
[3]*University of Illinois, Urbana-Champaign, Urbana, IL 61801.*

Abstract. Shock compression in nanocrystalline nickel is simulated over a range of pressures (10-80 GPa) and compared with experimental results. Laser compression carried out at Omega and Janus yields new information on the deformation mechanisms of nanocrystalline Ni. Although conventional deformation does not produce hardening, the extreme regime imparted by laser compression generates an increase in hardness, attributed to the residual dislocations observed in the structure by TEM. An analytical model is applied to predict the critical pressure for the onset of twinning in nanocrystalline nickel. The slip-twinning transition pressure is shifted from 20 GPa, for polycrystalline Ni, to 80 GPa, for Ni with g. s. of 10 nm. Contributions to the net strain from the different mechanisms of plastic deformation (partials, perfect dislocations, twinning, and grain boundary shear) were quantified in the nanocrystalline samples through MD calculations. The effect of release, a phenomenon often neglected in MD simulations, on dislocation behavior was established. A large fraction of the dislocations generated at the front are annihilated.

Keywords: laser shock, molecular dynamics, nanocrystalline metals, dislocations
PACS: 01.30.Cc, 62.50.-p.

INTRODUCTION

Molecular Dynamics (MD) simulations are well suited, both in time (~ns) and length scales (~100 nm), for comparison with laser-shock compression experiments and for providing insight on deformation processes involved. They have been extensively used for plastic deformation of nanocrystalline metals, e.g. [1]. Bringa et al. [2] studied shock compression of nc Cu. An increase in strength during shock loading was observed due to the suppression of grain-boundary sliding under compression by a Mohr-Coulomb-like mechanism. Both perfect and partial dislocations as well as nano-twins were observed in their simulations.

MD SIMULATIONS

The MD simulations were carried out using the Large-scale Atomic/Molecular Massively Parallel Simulator (LAMMPS) code [3]. EAM potentials for Ni (Mishin et al. [4]) and Cu (Mishin [5]) were used.

The 5nm grain-sized sample was subjected to piston velocities between 0.2 km/sec and 1.3 km/sec, and its Hugoniot was found to be very close to that of the monocrystalline sample. Figure 1 (b) provides an illustration of the shock wave for U_p ~1 km/sec as it traverses the sample. Since grain boundaries (i.e. defects) exist in the sample, the

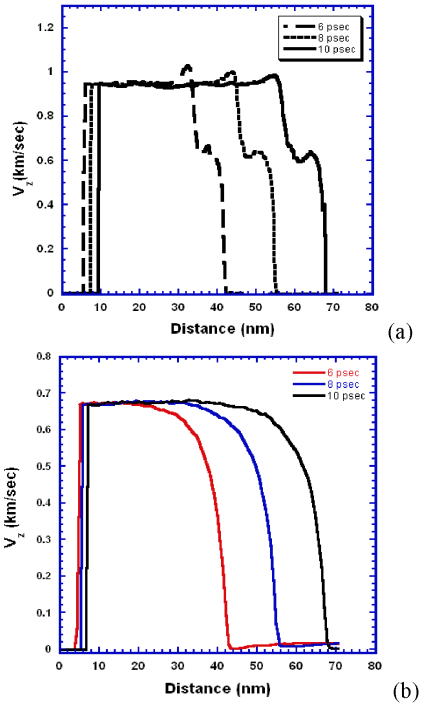

Figure 1. Piston/particle velocity at 6, 8 and, 10 psec versus distance (below the HEL) for P~35GPa;for (a) monocrystalline and (b) nanocrystalline Ni

HEL is lower than that in the single-crystal. A single-wave structure is evident and not a two-wave structure as seen in the single-crystalline results ([100]) shown in Fig. 1(a) for a pressure of 48GPa. This difference is attributed to the fact that the particle velocities vary in each individual grain, introducing fluctuations in the data that do not allow the plastic and elastic components to be resolved. In comparison with the single-crystal, the rise time is increased from ~ 2 nm to ~ 10 nm.

Figure 2 shows the generation of defects (primarily, partial dislocations) behind the front for the [100] monocrystal. Homogeneous dislocation loop generation in agreement with a model proposed earlier [6] and shown in Fig. 2(a) is the primary mechanism. Fig. 2(b) shows the generation of partial dislocation loops behind the front. In the absence of defects, they nucleate homogeneously.

The effect of loading and unloading on the deformation structure of nanocrystalline Ni was studied in the MD simulations to provide a more realistic comparison with the experiments. Figure 3 (b) shows a sequence of snapshots before, during, and after uniaxial compression. The loading history is shown in Fig. 3(a). At 14 ps, profuse partial dislocation generation from grain boundaries is seen. At 28 ps, after unloading, a significant fraction of these defects has disappeared. Grain boundaries act as sources and sinks for partial dislocations. Leading partials are mainly emitted from the grain boundaries, and trailing partials are seldom released. Limited evidence of twinning was also observed.

A quantitative analysis of the deformation mechanisms was carried out on three samples that were shocked using the same piston velocity of 0.67 km/sec (~ 38 GPa): 5 nm Ni, 10 nm Ni and 10 nm Cu. Figure 4 shows the three shocked samples. The color code is provided by Jarmakani et al.[7]; the dark atoms are not displaced and are in their original minimum energy state, and the light atoms are displaced by displaced by the Burgers vector of a Shockley partial (green), by the Burgers vector of a perfect dislocation (red), or by a Burgers vector larger than that of a perfect dislocation (orange). Contributions to the net strain from the various mechanisms of plastic deformation were

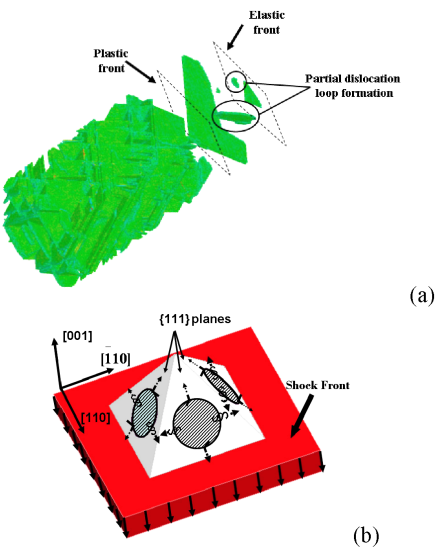

Figure 2. Shock compression of Ni along [001]; U_p=0.786 km/sec (a) Plastic zone formation; through formation of dislocation loops; (b) Homogeneous dislocation generation model [7].

TABLE 1. Strain contributions due to various mechanisms in MD specimens shocked at a piston/particle velocity of U_p=0.67 km/sec.

	Strain due to partial dis. (x 10^{-2})	Strain due to twinning (x 10^{-2})	Strain due to perfect dis. (x 10^{-2})	Total strain due to dislocation (x 10^{-2})	Grain-boundary shear (x 10^{-2})
Ni 5nm (shock)	1.18	0.355	0.142	1.38	11.6
Ni 5nm (shock-release)	0.73	0.29	0.182	1.0	-
Ni 10 nm (shock)	1.59	0.32	0.35	2.03	7.5
Cu 10 nm (shock)	1.64	0.42	0.45	2.18	7.5

calculated by determining the relative motion between nearest neighbor pairs of atoms, and resolving this motion along the strain axis. Table 1 lists the strains due to the different types of dislocations in the three samples. By subtracting the strain due to dislocations and twinning from the

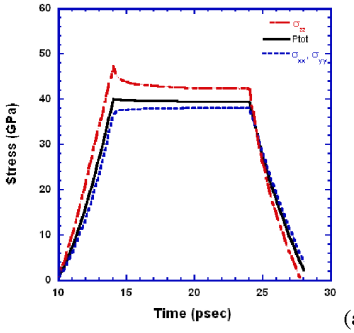

(a)

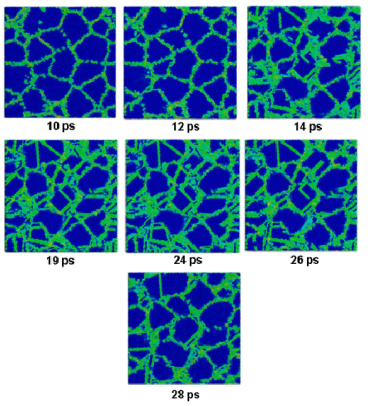

(b)

Figure 3. (a) Uniaxial compression and relaxation of 5nm grain sized Ni sample; (b) Frames at different times showing emission and annihilation by re-absorption of partial dislocations into grain boundaries position of shock front marked for the three samples).

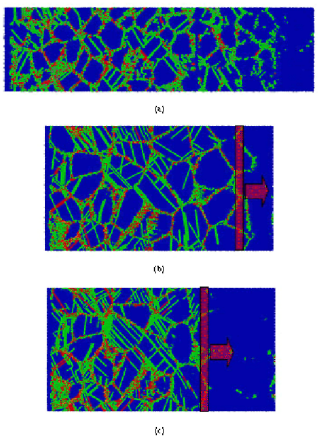

Figure 4. Comparison of deformation stucture for same particle velocity of U_p=0.67 mm/μsec (a) 5 nm Ni; (b) 10 nm Ni; (c) 10 nm Cu

total strain, one obtains the strain due to grain-boundary sliding; this represents approximately 90 % of the total for the 5 nm samples and 75% for the 10 nm sample, signifying that it becomes more difficult for larger grains to slide past one another under compression. Clearly, the total strain contribution due to dislocations is dominated by partials. The contribution due to twinning was 26 %. Perfect dislocations account for 17 % of the dislocation strain in Ni and 21 % in Cu. The twinning contribution is greater in Cu, 19 % as compared to 15.7 % in Ni. This is to be expected since the stacking fault energy of Cu is significantly lower.

Figure 5 is a Holian-Lomdahl [9] plot showing

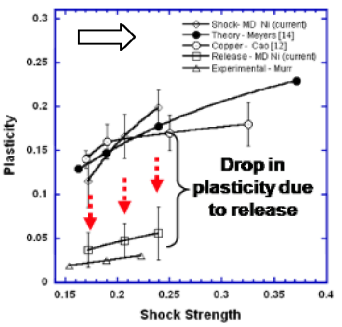

Figure 5. Holian-Lomdahl [9] plot showing Plasticity (=a_0/l) vs. Shock Strength(=U_p/C_o). Note difference between computed and measured values.

how plasticity (expressed as a_o/l; a_0 is the initial lattice parameter) varies with shock strength (U_p/C_0). The MD computations of several studies fall in the upper curve and are quite consistent with the homogeneous dislocation generation model [6]. On the other hand, the effect of stress release is dramatic. The experimental results by Murr (e. g. [8]) are much more consistent with the plasticity drop due to release.

EXPERIMENTAL RESULTS

The pre and post shock hardness of the Ni and Ni-W nanocrystalline specimens were measured. There is a clear increase in these values, which is dependent on the laser compression pressure. The results are shown in Figure 6. The experiments were performed at Janus with the use of a 1x1mm face plate to smooth out inhomogeneities in the laser beam. The addition of 13 wt. %W enabled smaller grain sizes, to ~10 nm because W pins the grain boundaries. TEM revealed that deformation twins were the predominant defect structures, in Ni-W shocked to 40 GPa, as indicated by circles in Figure 7(b). In contrast, Ni only exhibited dislocations (Fig. 7(a)).

A constitutive description of the onset of twinning

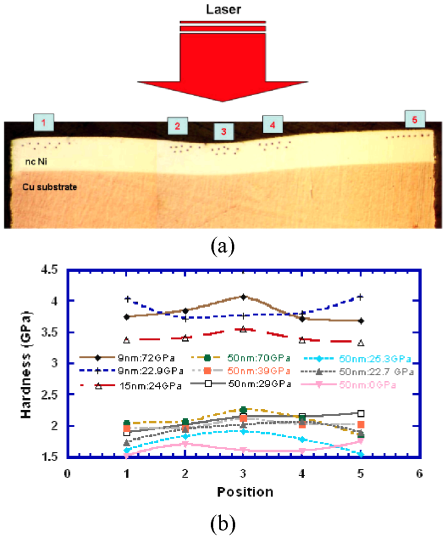

Figure 6. (a) Cross-sectional microhardness measurements from 5 positions beneath crater; (b) Hardness vs. position.

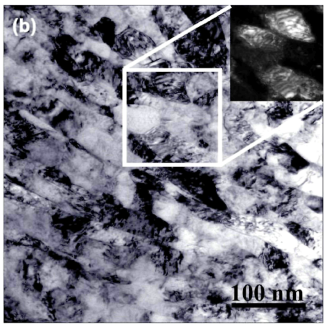

(a)

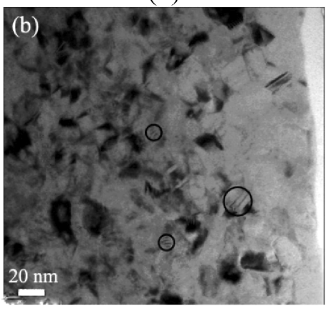

(b)

Figure 7. TEM of Ni with G. S. of 30-50 nm shocked at ~ 40 GPa showing dislocations; (b) TEM of Ni-W (13 at %) with G. S. of 10-15 nm shocked at ~ 40 GPa; deformation twins are evident (circles).

in nanocrystalline nickel and nickel-tungsten subjected to shock compression was developed. It is described in detail by Jarmakani et al. [7]. We assume that slip and twinning are competing processes and that the onset of twinning occurs when the shear stress for twinning, τ_T , becomes equal to or less than the shear stress for slip, τ_S :

$$\tau_T \leq \tau_S \qquad (1)$$

Dislocation motion is very sensitive to strain rate and temperature, whereas twinning is much less sensitive. Thus, the twinning stress was assumed to be independent of temperature and strain rate. The effect of grain size on the twinning stress has been found to be greater than that on the slip stress for many metals and alloys. A Hall-

Petch relationship can, thus, be ascribed to the twinning stress, with $k_t \sim 3k_s$.

Solid-solution strengthening and stacking-fault energy effects are incorporated into the slip-twinning model as a result of alloying with tungsten. Alloying significantly increases the yield stress and reduces the stacking fault energy, γ_{sf}. The twinning stress, τ_T, varies with stacking-fault energy, γ_{sf} in the following form:

$$\tau_T = k\left(\frac{\gamma_{sf}}{Gb_S}\right)^{1/2} \qquad (2)$$

where k is a proportionality constant, b_s is the Burgers vector, and G is the shear modulus. Eqn. 2 has been incorporated into our analysis.

The slip behavior of Ni is modeled as a function of shock pressure, temperature, strain, and strain-rate. The Hall-Petch slope for slip was taken as $k_S \sim 0.2$ MN/m$^{3/2}$. The Zerilli-Armstrong equation as a function of tungsten content is obtained by adding the solid-solution term into the athermal component of stress (first term in Eqn. 3):

$$\sigma_{slip} = \sigma_G + (\sum_i K_i^{1/m} C_i)^m + C_2 \varepsilon^n \exp(-C_3 T + C_4 T \ln\dot{\varepsilon}) + k_s d^{-1/2} \quad (3)$$

The strain-hardening exponent n of the nc Ni samples was simply equated to 0 as determined by measurements carried out on the same material. C_i is the effect of solutes. The values of C_3 and C_4 used are those for copper since data on Ni was not available. Stress-strain plots of nickel with micrometer sized grains were utilized to establish C_2. The model predicts a yield strength of ~ 1.9 GPa for Ni having a grain size of 30 nm, in agreement with the literature.

The twinning H-P slope was assumed to be 0.6 MN/m$^{3/2}$. Ni twins at 4.2 K and 20 K at a shear stress equal to 250-280 MPa, which is equivalent to a normal stress of 500-560 MPa. The following expression for the twinning stress was applied:

$$\sigma_T = k\left(\frac{\gamma_{sf}}{Gb_S}\right)^{1/2} + k_{T_{NiW}} d^{-1/2}$$

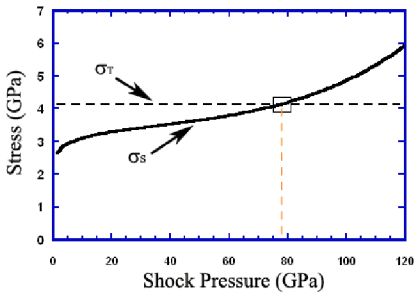

(a)

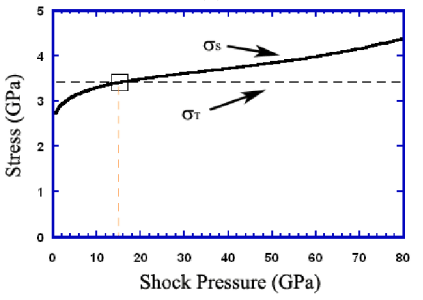

(b)

Figure 8. Slip and twinning stress vs. shock pressure for nanocrystalline (a) nickel (G. S. = 30nm); (b) Ni-W (13. at. %) (G. S. =10nm).

The dependence of shock pressure on strain rate for Ni, obtained through the Swegle-Grady relationship [10], is approximated as:

$$\dot{\varepsilon} = 7.84\times10^{-33} \times P_{shock}^{\ 4} \qquad (4)$$

Two separate aspects have to be considered in the analysis: (a) plastic strain at the shock front and (b) shock heating. Both plastic strain by slip (and associated work hardening) and shock heating alter the flow stress of a material by slip processes and need to be incorporated into the computation. The total (elastic + plastic) uniaxial strain, ε, at the shock front is related to the change in specific volume by:

$$\frac{V}{V_0} = e^{\varepsilon} \qquad (5)$$

The pressure dependence of strain, determined from the Rankine-Hugoniot equations and equation of state, and Eqn. 5, is expressed as follows:

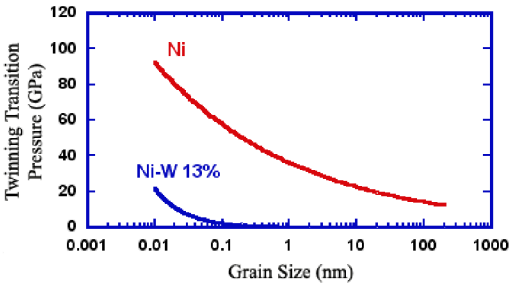

Figure 9. Calculated twinning-transition pressure vs. grain size for Ni and Ni-13 at. %W.

$$P_{shock} = \frac{C_0^2(1-e^{\epsilon})}{V_o[1-S(1-e^{\epsilon})]^2} \qquad (6)$$

The associated temperature rise in Ni as a function of shock pressure is represented by Eq. 7, which is a polynomial that was generated from thermodynamically calculated data:

$$T_{shock} = 8\times10^{-20}\times P_{shock}^{\ 2} + 9\times10^{-10}\times P_{shock} + 301.5 \text{ K} \qquad (7)$$

Figure 8 shows both the slip stress, (incorporating thermal softening, strain-rate hardening, and work hardening) and the twinning stress as a function of pressure. The point at which the twinning stress intersects the slip stress is defined as the critical twinning transition pressure. This transition pressure for nickel having G. S.=30 nm was found to be 78 GPa (Fig. 8(a)), and is consistent with the fact that twins are not observed in experiments up to pressures of ~70 GPa. For Ni-W, this transition is reduced to 16 GPa, for a G. S. =10 nm; this is also consistent with observations (Fig. 7).

The twinning-transition pressure as a function of grain size is shown in Figure 9. It clearly shows the much higher transition pressures in Ni as compared to Ni-W as well as the effect of grain size on the slip-twinning transition.

CONCLUSIONS

1. Grain-boundary sliding is the major deformation mechanism for shock compression of nanocrystalline Ni and Cu. Partial dislocations dominate the slip component of strain. Grain-boundary sliding was found to be slightly less for the 10 nm G. S. More twinning was also favored for the smaller Ni (5nm) G. S. as compared to the 10nm G. S. .

2. Upon unloading, reabsorption of partials was observed. This could explain the differences between experimentally observed and computed (analyrtically or by MD) dislocation densities.

3. An analytical model for the slip-twinning transition in nanocrystalline nickel (GS ~30 nm) is presented. For Ni, a critical twinning pressure of 78 GPa is predicted, consistent with TEM observations. For Ni-W (G. S. ~10 nm) the critical twinning pressure is 16 GPa, also consistent with TEM observations.

Acknowledgements: This work was funded by the UCOP ILSA contract No. W-7405-Eng-48. The help provided by Dr. D. Correll is gratefully acknowledged. Parts of this work were also supported by U.S. DOE-BES, under Grant No. DEFG02-91ER45439. We thank Prof. C. Shuh for providing the nanocrystalline material.

REFERENCES

1. Van Swygenhoven H., Caro A., Phys. Rev. B, 58, 11246, 1998.
2. Bringa E. M., Caro A., Wang Y., Victoria M., McNaney J. M., Remington B. A., Smith R. F., Torralva B. R., Van Swygenhoven H., Science, 309, 1838, 2005.
3. Plimpton S. J., J. Comput. Phys., 117,1-19, 1995 (http://lammps.sandia.gov)
4. Mishin Y., Farkas D., Mehl M. J., Papaconstantantopoulos D. A., Phys. Rev. B, 59, 3393, 1999.
5. Mishin Y., Mehl M. J., Papaconstantopoulos D. A., Voter A. F., Kress J. D., Phys. Rev. B, 63, 224106, 2001.
6. Meyers M. A., Scripta. Metall. 12, 21, 1978.
7. Jarmakani H., ,Bringa E. M., Erhart P., Wang Y. M., Vo N. Q., Meyers M. A., Acta. Mat., 56, 5584, 2008.
8. Murr L. E., "Shock Waves and High-Strain Rate Phenomena in Metals", Plenum. Press., New York, NY, pp. 607, 1981.
9. Holian B. L., Lomdahl P. S., Science, 10, 2085, 1998.
10. Swegle J. W., Grady D. E., "Shock Waves in Condensed Matter-1985", eds. Y. M. Gupta, Plenum, New York, pp. 353, 1986.